

Signature of systemic rotation in 21 Galactic Globular Clusters from APOGEE-2

Ilaria Petralia¹, Dante Minniti^{1,2,3}, José G. Fernández-Trincado⁴, Richard R. Lane⁵, and Ricardo P. Schiavon⁶

¹ Instituto de Astrofísica, Facultad de Ciencias Exactas, Universidad Andrés Bello, Fernández Concha 700, Las Condes, Santiago, Chile

e-mail: ilariapetralia28@gmail.com

² Vatican Observatory, Vatican City State, V-00120, Italy

³ Departamento de Física, Universidade Federal de Santa Catarina, Trindade 88040-900, Florianópolis, Brazil

⁴ Instituto de Astronomía, Universidad Católica del Norte, Av. Angamos 0610, Antofagasta, Chile

⁵ Centro de Investigación en Astronomía, Universidad Bernardo O'Higgins, Avenida Viel 1497, Santiago, Chile

⁶ Astrophysics Research Institute, Liverpool John Moores University, 146 Brownlow Hill, Liverpool L3 5RF, UK

April 18, 2024

ABSTRACT

Context. Traditionally, Globular Clusters (GCs) have been assumed to be quasi-relaxed nonrotating systems, characterized by spherical symmetry and orbital isotropy. However, in recent years, a growing set of observational evidence is unveiling an unexpected dynamical complexity in Galactic GCs. Indeed, kinematic studies show that a measurable amount of internal rotation is present in many present-day GCs.

Aims. The objective of this work is to analyse the APOGEE-2 Value-Added Catalogs (VACs) DR17 data of a sample of 21 GCs to extend the sample showing signatures of systemic rotation, in order to better understand the kinematic properties of GCs in general. Also, we aim to identify the fastest rotating GC from the sample of objects with suitable measurements.

Methods. From the sample of 23 GCs included in this work, the presence of systemic rotation was detected in 21 of the GCs, using three different methods. All these methods use the radial velocity referred to the cluster systemic velocity (\tilde{V}_r). Using the first method, it was possible to visually verify the clear-cut signature of systemic rotation. Whereas, using the second and third methods, it was possible to determine the amplitude of the rotation curve (A_{rot}) and the position angle (PA) of the rotation axis.

Results. This study shows that 21 GCs have a signature of systemic rotation. For these clusters, the rotation amplitude and the position angle of the rotation axis (PA_0) have been calculated. The clusters cover a remarkable range of rotational amplitudes, from 0.77 km/s to 13.85 km/s.

Key words. Globular clusters: general – Stars: kinetics and dynamics

1. Introduction

Galactic globular clusters (GCs) represent one of the ideal laboratories to study stellar dynamics and its effects on stellar evolution. Traditionally, GCs have been assumed to be quasi-relaxed nonrotating systems, characterized by spherical symmetry and orbital isotropy. Spherical isotropic (King 1966) and non-rotating (Wilson 1975) models have indeed been shown to provide a satisfactory zeroth-order description of the main observed dynamical properties.

However, in recent years, a growing set of observational evidence is unveiling an unexpected dynamical complexity in Galactic GCs, demonstrating that the traditional assumptions of sphericity, pressure isotropy and nonrotation are far too simplistic. In fact, kinematic studies show that a significant amount of internal rotation is present in many present-day Milky Way (MW) GCs (Lane et al. 2011; Bellazzini et al. 2012; Bianchini et al. 2013; Fabricius et al. 2014; Kacharov et al. 2014; Kimmig et al. 2015; Lardo et al. 2015; Bellini et al. 2017; Boberg et al. 2017; Jeffreson et al. 2017; Cordero et al. 2017; Lee 2017; Ferraro et al. 2018; Kamann et al. 2018; Lanzoni et al. 2018; Bianchini et al. 2018; Szigeti et al. 2021). All these results suggest that, since it is possible to study individual stellar components individually, the vast majority of GCs show

signatures of the presence of internal rotation.

This observational evidence plays a fundamental role to construct a complete dynamical picture of GCs. Indeed, the presence of a significant amount of internal rotation raises a series of fundamental issues connected to the formation and evolution of GCs and the different dynamical processes involved (e.g., Giersz & Heggie 2011). For instance, many studies indicate that rotation accelerates evolution (e.g. Einsel & Spurzem 1999; Kim et al. 2008; Hong et al. 2013) and strongly shapes their present-day morphology (van den Bergh 2008; Bianchini et al. 2013). Moreover, the present-day signatures could be the relic of a stronger internal rotation set at the epoch of the cluster's formation (Vesperini et al. 2014; Lee & Henebelle 2016; Mapelli 2017; Tiongco et al. 2017) or indicate a peculiar evolutionary environment (Lane et al. 2010a, Vesperini et al. 2014; Tiongco, Vesperini, & Varri 2018). Signatures of internal rotation could also be crucial in the kinematical differences between multiple stellar populations (Richer et al. 2013; Bellini et al. 2015; Cordero et al. 2017; Bellini et al. 2018; Cordonì et al. 2020a, 2020b; Dalessandro et al. 2021; Libralato et al. 2023). As a result of these interesting studies, new theoretical models are being developed. Of great interest is the proposed new distribution-function-based models of rotating

and anisotropic models (see, e.g., Varri & Bertin 2012; Gieles & Zocchi 2015; de Vita et al. 2016), expanding the traditional model. Several numerical simulations have also been carried out to understand the rotational properties of GCs (see, e.g. Einsele & Spurzem 1999; Ernst et al. 2007; Livernois et al. 2021, 2022, Kamlah et al. 2022, Tiongco et al. 2022). One of these was the starting point to find the first observational evidence of a relation between globular clusters' internal rotation and stellar masses (Scalco et al. 2023). As shown from these theoretical studies, the presence of internal rotation has several implications for the long-term dynamical evolution of clusters (e.g. the observed GC rotation may be a lower limit to a GC's initial rotation due to angular momentum loss during its evolution).

In this work, the kinematic analysis for 23 Galactic GCs is presented, in order to verify the presence of a systemic rotation in these objects. This study is based on the individual radial velocities of stars available for each individual cluster. The data used come from the high-resolution spectroscopic survey Apache Point Observatory Galactic Evolution Experiment (APOGEE; Majewski et al. 2016). The astrometric parameters, such as position (RA and DEC, see Vasiliev & Baumgardt 2021), the abundances and the radial velocity referred to the cluster systemic velocity (\tilde{V}_r) were previously calculated for all stars (see Schiavon et al. 2023). For this reason, the available catalogue represents a good sample to study.

The present work is structured as follows. In Section 2 we present the data available for the sample GCs, that were employed in the calculations. Section 3 includes a kinematics analysis, while in Section 4 the results are summarized and discussed, and conclusions are drawn in Section 5.

2. Available data

The data used to conduct this analysis were collected from two different catalogues. The first one is a list of globular cluster (GC) star members from the latest data release of the SDSS-IV/APOGEE-2 survey (DR17¹, Majewski et al. 2017; Abdurro'uf et al. 2022). Cluster membership is based on a combination of position, proper motion, radial velocity, and metallicity cuts obtained using data from both the APOGEE-2 (DR17) and Gaia (EDR3) surveys (Gaia Collaboration et al. 2021). Whereas, the second one contains the global parameters adopted for globular clusters included in the cluster member Value-Added Catalogs (VACs) generated from APOGEE-2 DR17 (Schiavon et al. 2023).

The list of GCs and their characteristics considered in this work is shown in Table 1. This table lists the GC positions, number of stars, velocity dispersion, fitted and peak-to-peak amplitudes, and position angles. The number of stars observed varies from cluster to cluster, but each cluster has at least 60 stars available. In general, the number of observed stars varies from 65 to 1864. We emphasize that the number of available stars for each cluster doubles the previous APOGEE sample. Further details about these APOGEE-2 data and their acquisition and reduction techniques and the criteria adopted for selecting candidate GC members are presented in Schiavon et al. 2023.

3. Kinematic analysis

Among the various available parameters, of particular importance for this analysis is the radial velocity referred to the cluster

systemic velocity (\tilde{V}_r), namely the difference between the radial velocity of star (V_r) and the systemic velocity of the GC (V_{sys}) in units of the adopted radial velocity dispersion (σ_{rv})² (see equation 1).

$$\tilde{V}_r = (V_r - V_{sys}) \quad [\text{km/s}] \quad (1)$$

Indeed, all methods used in this work to check the presence of rotation in GCs are based on \tilde{V}_r .

A quick and visually efficient method to check for systemic rotation in GCs is to use the distribution of the stars with different V_r on the plane of the sky (Figure 1), with the red and the blue colors indicating, respectively, positive and negative values of \tilde{V}_r (i.e., V_r larger and smaller than the systemic velocity, respectively). As apparent from the figure, the evident prevalence of stars with positive values of \tilde{V}_r in the lower-left portion of the map and that of sources with $\tilde{V}_r < 0$ in the upper-right part of the diagram is a clear-cut signature of systemic rotation.

To investigate the rotation in GCs, we used the same method, as was adopted by Cote et al. 1995, Pancino et al. 2007 and Lane et al. 2010b and fully described in Bellazzini et al. 2012 and Lanzoni et al. 2013. For any given cluster, the method consists in splitting the sample in two, by considering a line passing through the cluster center with position angle (PA) varying between 0° (north direction) and 90° (east direction), using steps of 18°³, clockwise system⁴. For each value of the PA, the difference $\Delta < \tilde{V}_r >$ between the mean radial velocity of the two sub-samples was computed and it is plotted as a function of the PA (see, for example, Figure 2). Its coherent sinusoidal behavior is a signature of rotation and the parameters of the best-fit sine function provide us with the amplitude of the rotation curve and the PA of the rotation axis (for the exact meaning of this parameter see the discussion in Bellazzini et al. 2012). The observed patterns were fitted with the sine law, which provides a reasonable fit to the data, and is shown in equation 2:

$$\Delta < \tilde{V}_r > = dist + A_{rot} \cdot \sin(\omega \cdot PA + \phi) \quad (2)$$

where $dist$ is the displacement, ω is frequency, ϕ is the phase of the best-fit sine function⁵. A_{rot} is the rotation amplitude, which is two times the actual mean amplitude, because it is the difference of the two hemispheres (in km/s). The minimum and maximum position in the best-fit sine function is the position angle of the dividing line corresponding to the maximum rotation amplitude (in degrees), coinciding with the rotation axis. It should be noted, however, that the values of the PA of the rotational axis (PA_0) given in the Table 1 are indicative estimates of the actual values.

² In this work, the adopted radial velocity dispersion values are referred to global dispersion.

³ This value is the same for all GCs studied and was chosen to divide the range of PA values equally and while at the same time considering a significant number of stars for each range in order to perform the analysis described. More detail explaining the choice of using this step value is shown in Appendix C.

⁴ This convention is different from that used in reference works that adopt the same analysis methodology. Thus, to compare our results with those of literature works, we convert and report the values into the reference notation, namely PA 90 = East, anti-clockwise system.

⁵ The values of $dist$, ω , ϕ have no relevance for the kinematic analysis in this work, but these coefficients are only relevant in the computational part. Indeed, they were included in the formula only to improve and find the best-fit sine function.

¹ <https://www.sdss4.org/dr17>

Table 1. Summary of GCs analysed in this work. The target names and their coordinates of GC centre from Vasiliev & Baumgardt 2021 catalogue are listed in columns 1-4. The Jacobi radius for each cluster is listed in the fifth column. The number of stars available for the various clusters is shown in the sixth column, while the seventh column contains the adopted radial velocity dispersion. The eighth and ninth columns show the rotation amplitude values calculated using the best-fit sine function method and the peak-to-peak method respectively. The tenth column shows the values of the PA of the rotation axis, following the methodology used to calculate A_{fit} . These values were converted and reported into PA 90 = East, anti-clockwise system. Finally, in the last column, the values of V/σ (or A_{fit}/σ_{rv}) calculated for each cluster. The last two GCs are clusters that do not show signature of systemic rotation.

Object		RA_0 [deg]	DEC_0 [deg]	r_J [deg]	N_*	σ_{rv} [km/s]	A_{fit} [km/s]	$A_{peak-peak}$ [km/s]	PA_0 [deg]	A_{fit}/σ_{rv}
NGC 0104	47 Tuc	6.02379	-72.08131	1.557	302	12.0	9.16 ± 0.50	12.41 ± 0.39	216	0.76
NGC 0362		15.80942	-70.84878	0.598	70	8.6	3.57 ± 0.08	3.63 ± 0.88	234	0.42
NGC 1851		78.52816	-40.04655	0.611	71	11.0	5.59 ± 0.13	5.94 ± 5.84	180	0.51
NGC 2808		138.01291	-64.86349	0.944	132	14.1	8.42 ± 0.34	8.29 ± 1.00	198	0.60
NGC 3201		154.40343	-46.41248	0.925	217	4.7	3.37 ± 0.10	3.88 ± 0.26	324	0.72
NGC 5139	ω Cen	201.69699	-47.47947	2.142	1864	17.7	13.85 ± 0.25	12.98 ± 0.29	162	0.78
NGC 5272	M 3	205.54842	28.37728	0.714	299	7.8	2.46 ± 0.12	2.85 ± 0.40	162	0.32
NGC 5904	M 5	229.63841	2.08103	0.607	259	7.8	8.03 ± 0.14	7.88 ± 0.74	198	1.03
NGC 6121	M 4	245.86974	-26.52575	1.658	224	4.8	2.70 ± 0.08	3.16 ± 0.15	234	0.56
NGC 6171		248.13275	-13.05378	0.368	65	4.1	0.77 ± 0.09	1.38 ± 0.34	234	0.19
NGC 6205		250.42181	36.45986	1.036	152	9.6	5.62 ± 0.17	6.03 ± 0.72	306	0.59
NGC 6254	M 10	254.28772	-4.10031	0.611	87	6.3	2.27 ± 0.16	3.74 ± 0.46	198	0.36
NGC 6273		255.65749	-26.26797	0.266	81	12.1	2.37 ± 0.22	3.78 ± 2.32	270	0.20
NGC 6341		259.28076	43.13594	0.808	80	8.7	4.18 ± 0.11	5.31 ± 0.91	216	0.48
NGC 6388		264.07178	-44.7355	0.516	75	17.4	6.64 ± 0.47	11.68 ± 2.58	270	0.38
NGC 6397		265.17538	-53.67434	1.174	187	5.5	1.39 ± 0.08	1.93 ± 0.64	198	0.25
NGC 6656	M 22	279.09976	-23.90475	1.308	412	8.9	5.75 ± 0.06	6.24 ± 0.98	252	0.65
NGC 6715	M 54	283.76385	-30.47986	0.618	1809	19.2	6.01 ± 0.18	8.20 ± 0.57	252	0.31
NGC 6752		287.7171	-59.98455	0.913	152	7.7	1.04 ± 0.15	1.19 ± 0.34	162	0.14
NGC 6809		294.99878	-30.96475	0.549	98	4.9	3.58 ± 0.10	3.35 ± 0.28	252	0.73
NGC 7078	M 15	322.49304	12.167	0.757	155	13.0	4.16 ± 0.10	4.83 ± 1.45	234	0.32
NGC 6218		251.80907	-1.94853	0.508	107	4.8	-	-	-	-
NGC 6838		298.44373	18.77919	0.619	129	2.7	-	-	-	-

The rotation amplitude derived from the best-fit function for all GCs (A_{fit}) is shown in Table 1, while the observed patterns with the best-fit sine function of all GCs are shown in Figure 3 and 4. In this work, another method was also used to calculate the rotation amplitude, namely the peak-to-peak approach. In this case, the values of absolute minimum and absolute maximum of $\Delta < \tilde{V}_r >$ among all the observed patterns are identified and the amplitude of the rotation is the difference between the maximum value and the minimum value, namely $A_{rot} = \Delta < \tilde{V}_r >_{max} - \Delta < \tilde{V}_r >_{min}$. The rotation amplitude obtained from this method for all GCs ($A_{peak-peak}$) is shown in Table 1.

3.1. Measurement of uncertainties

As regards the best-fit sine function method, we derive the rotation amplitude and its uncertainty using the SCIPY⁶ package of PYTHON. Indeed, this package allows us to derive the parameters of the best-fit sine function, such as the rotation amplitude, and their uncertainties. Whereas, in the case of the peak-to-peak approach, the measurement of uncertainties of the rotation amplitudes was calculated starting from the uncertainties of the radial velocities of each star member of the cluster and the uncertainty of the systemic velocity of the cluster and considering the propagation of these uncertainties. The final value of uncertainty of rotation amplitude is given by the

⁶https://docs.scipy.org/doc/scipy/reference/generated/scipy.optimize.curve_fit.html

quadrature sum of the uncertainties of the observed patterns. As can be noted from the results reported in the Table 1, the values of the uncertainty calculated for the peak-to-peak approach are slightly high, especially for some clusters with a low number of available stars.

In general, the APOGEE velocities are good to < 1 km/s, thus excluding the individual stars with large radial velocity errors does not show a large difference with the results reported.

4. Results and Discussion

In this work, 23 GCs were studied in order to reveal a possible presence of systemic rotation. In this analysis, the rotation patterns were detected from radial velocities. Note that the rotation amplitudes detected from V_r samples are just lower limits to the true 3D amplitude, because of projection onto the plane of the sky (Bellazzini et al. 2012). Moreover, it must also be noted that the amplitude generally varies significantly with distance from the cluster center (see, for example, the case of ω Cen Sollima et al. 2009), but the A_{rot} , derived using the full range of radius, is a reasonable proxy for the actual maximum amplitude (see Pancino et al. 2007).

As a main result, we find that 21 GCs show a systemic rotation and cover a remarkable range of rotational amplitudes, from ~ 0.77 km/s to ~ 13.85 km/s. For these clusters, we have also derived the PA of the rotation axis. The A_{rot} and PA_0 values of

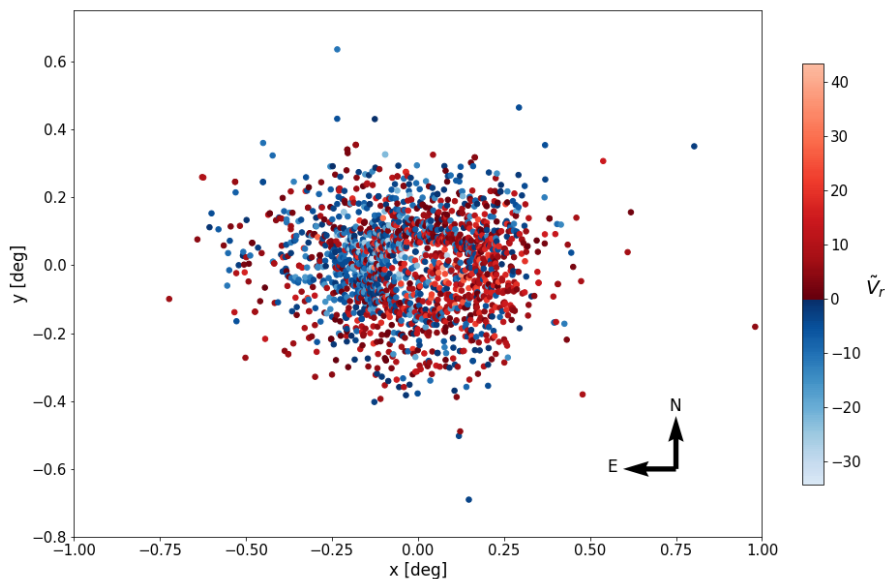


Fig. 1. Distribution of the observed sample on the plane of the sky of NGC 5139, with $x = (RA_0 - RA) \cdot \cos(DEC)$ and $y = DEC - DEC_0$ (RA_0 and DEC_0 being the coordinates of the cluster center, adopted from Vasiliev & Baumgardt 2021 catalogue). The colors distinguish stars with radial velocities referred to the cluster systemic velocity (\tilde{V}_r) > 0 (in red), from those with $\tilde{V}_r < 0$ (in blue). Black arrow vectors indicate the north (N) and east (E) direction.

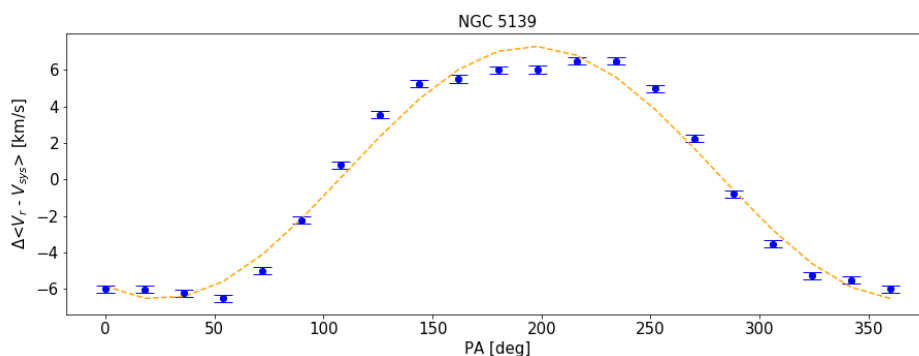


Fig. 2. Difference between the mean radial velocities located on each side of the cluster with respect to a line passing through the center as a function of PA (measured from north, PA = 0°, to east, PA = 90°, clockwise system) as a function of the adopted PA, for the globular cluster NGC 5139. The orange dashed line is the sine function that best fits the observed patterns (blue dots).

these clusters are shown in Table 1.

Once the clusters that show the signature of systemic rotation have been detected and their A_{rot} and PA_0 have been calculated, we have identified the fastest rotating GCs in our sample. As reported in Bellazzini et al. 2012, Kacharov et al. 2014 and Alfaro-Cuello et al. 2020, the parameter A_{rot}/σ (or with the most commonly used nomenclature V/σ), namely the rotation amplitude divided by velocity dispersion of the cluster, can be used for this purpose. Indeed, this parameter is expected to capture the relevance of rotation with respect to random motions. In this work, the parameter A_{rot}/σ was calculated using the rotation amplitude derived from the best-fit sine function and the adopted radial velocity dispersion (A_{fit} and σ_{rv} in the Table 1). In Table 1, the values of this parameter are shown for each cluster of the sample. According to the results obtained, the fastest GCs are NGC 5904, NGC 5139 and NGC 0104.

As a final analysis, a comparison between the rotation amplitude values obtained from the best-fit sine function of the observed patterns and the rotation amplitude values derived from the peak-to-peak method was made. As can be seen in the Table 1, the calculated amplitudes are within the uncertainties of each other, but in some cases, there are significant differences between the two methods (e.g. 6.64 km/s versus 11.68 km/s for NGC 6388). Moreover, for a few GCs, the peak-to-peak approach returns slightly high uncertainty values. The result of this comparison is shown in Figure 5. In this figure, the values of A_{fit} and $A_{peak-peak}$ (black dots) for each GCs were plotted and a linear regression was performed to find the line that best fit the data (red line). As a result, the best-fit line is:

$$A_{peak-peak} = 1.0 \cdot A_{fit} + 0.8 \quad (3)$$

Consequently, due to the slightly high uncertainty values from the peak-to-peak approach for a few GCs, the derivation of rotation amplitude from the best-fit sine function method is the

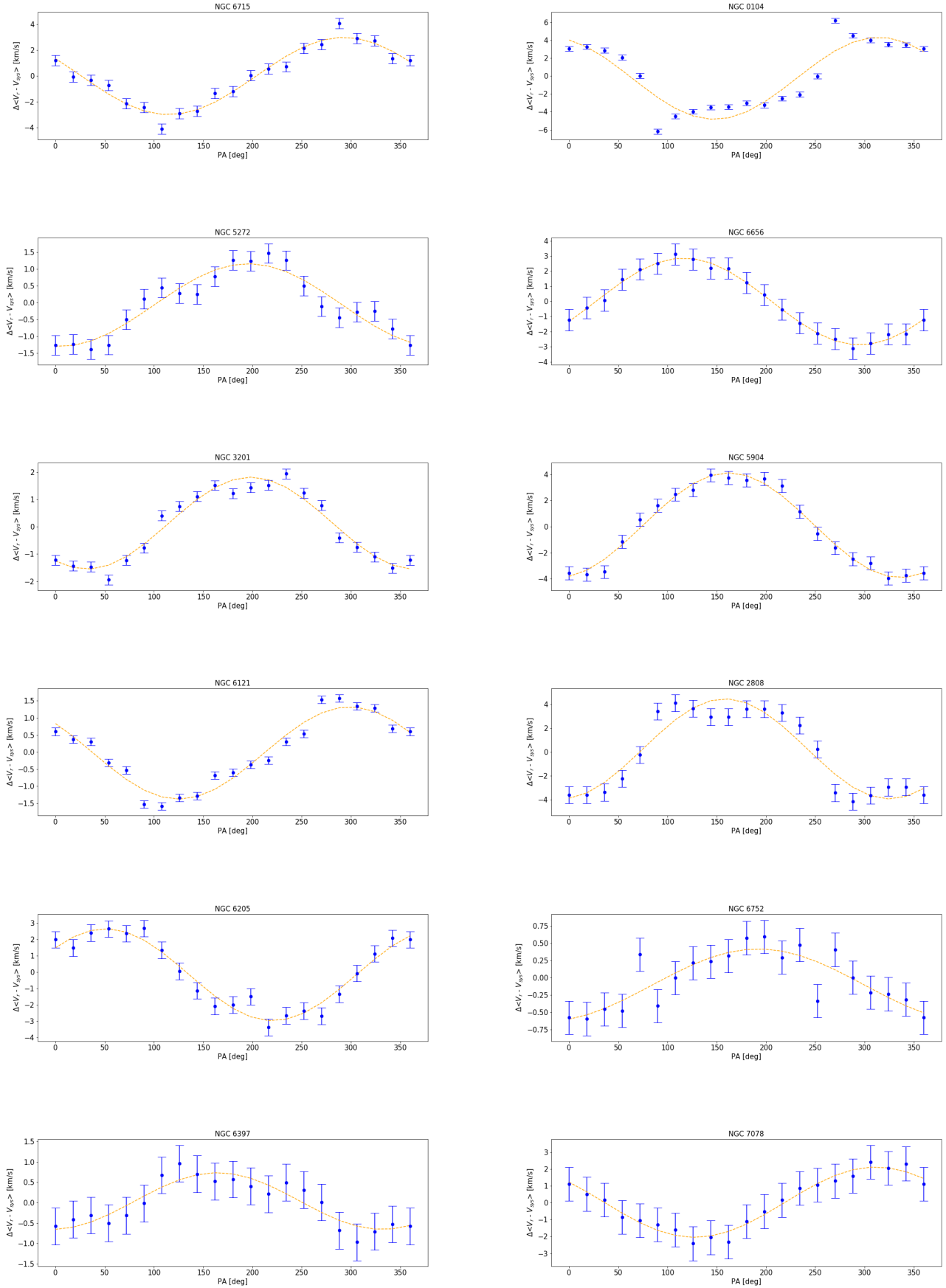


Fig. 3. Signature of systemic rotation for globular clusters NGC 6715, NGC 0104, NGC 5272, NGC 6656, NGC 3201, NGC 5904, NGC 6121, NGC 2808, NGC 6205, NGC 6752, NGC 6397 and NGC 7078.

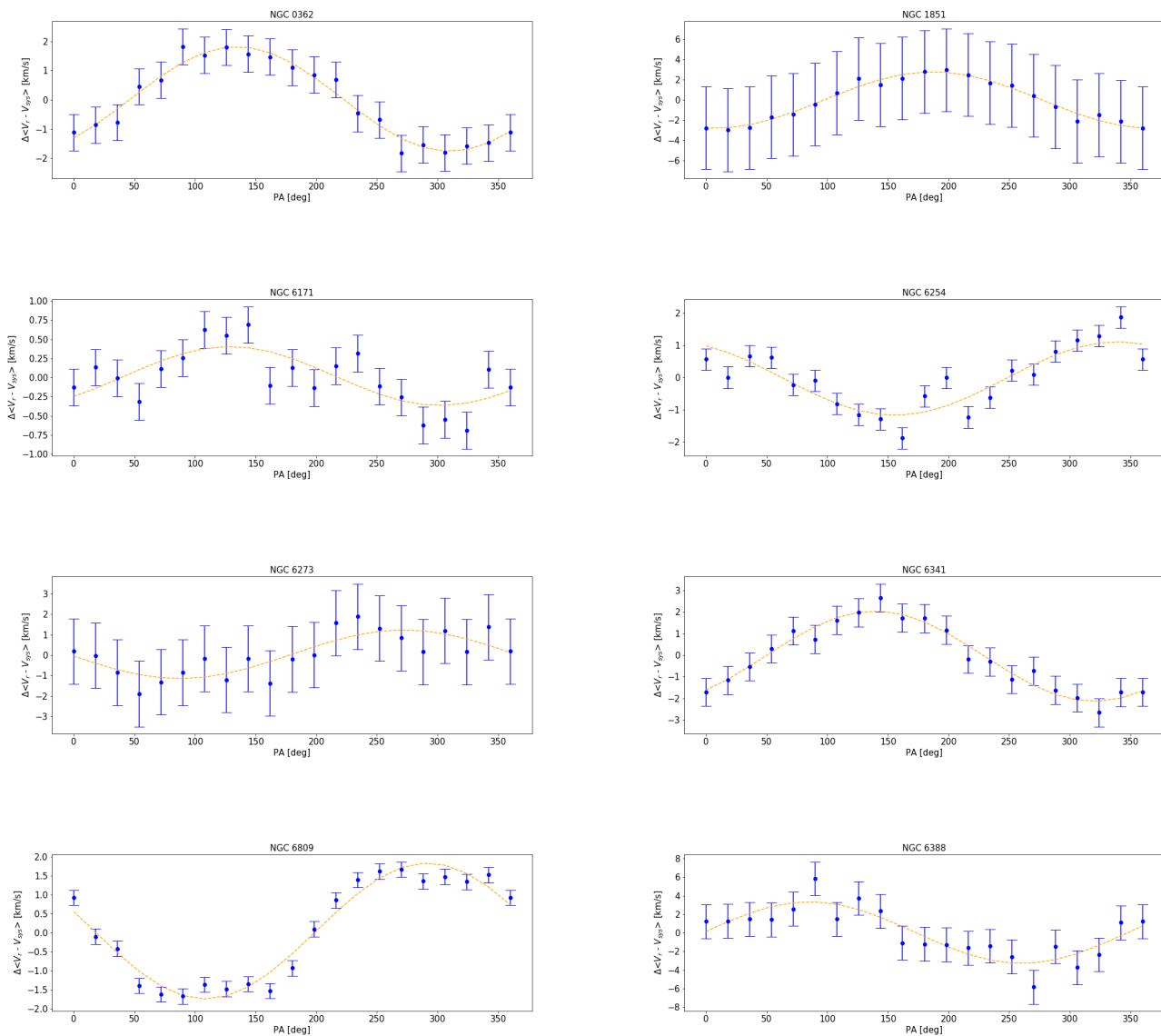


Fig. 4. Signature of systemic rotation for globular clusters NGC 0362, NGC 1851, NGC 6171, NGC 6254, NGC 6273, NGC 6341, NGC 6809 and NGC 6388.

most accurate. However, given the best-fit equation, it can be concluded that the use of the two methods gives equivalent results. Indeed, both methods can be considered two good tools for determining the rotation amplitudes.

4.1. Comparison with literature

The signature of systemic rotation for these GCs is consistent with the works of Lane et al. 2010b, Bellazzini et al. 2012, Fabricius et al. 2014; Cordero et al. 2017; Johnson et al. 2017, Kamann et al. 2018, Bianchini et al. 2018, Ferraro et al. 2018, Lanzoni et al. 2018, Sollima et al. 2019 and Szigeti et al. 2021. Among these, of particular interest are the work of Lane et al. 2010b, Bellazzini et al. 2012, Bianchini et al. 2013; Lardo et al. 2015; Kimmig et al. 2015; Lee 2017; Ferraro et al. 2018 and Lanzoni et al. 2018, because they used the same method as in this work to analyse the same clusters, and the work of Szigeti et al. 2021 because they used data from APOGEE-2 survey. Since all clusters have been studied in the literature before, it

is possible to compare the results of the present homogeneous sample with these other previous studies. The latest results available in the literature were collected in Table 2, which contains the calculated rotation amplitude and position angles of the rotational axis. Since multiple conventions are used in the literature for angle and direction notations (e.g. in the work of Fabricius et al. 2014; Cordero et al. 2017; Kamann et al. 2018 and Sollima et al. 2019), the published results have been converted the PA $90 = \text{East}$ convention, anti-clockwise system. The conversion of the PA_0 values of these works can be found in the appendix A. The PA_0 values measured in this work and shown in Table 1 have also been converted. To convert the values into the reference notation, a subtraction was performed between 360° and the measured PA_0 value for each cluster.

As reported above, one of the most relevant works with which to compare the results is the study of Szigeti et al. 2021, because also in this work APOGEE data have been used. However, our study shows some differences in terms of available data. The

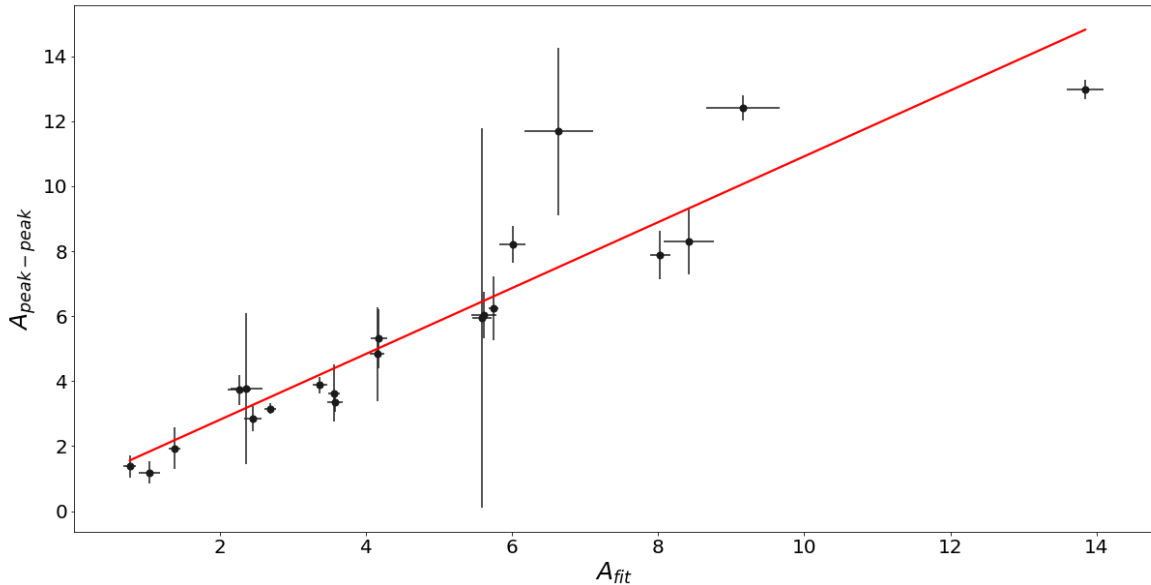


Fig. 5. Comparisons of rotation amplitude values obtained from the sinusoidal best-fit function and the peak-to-peak approach. The black dots are the values of the rotation amplitude for each GCs, while the red line is the best-fit line obtained from the linear regression.

first difference is that Szigeti et al. 2021 used the DR14 data release of APOGEE (Holtzman et al. 2018), while we used the expanded DR17 data release of APOGEE (Schiavon et al. 2023). Two other differences are the number of GCs analysed and the stars observed for each individual cluster. Indeed, Szigeti et al. 2021 studied a total of 10 GCs, but they were able to successfully measure the rotation speed and position angle of the rotation axis for 9 clusters. Instead, in our work, we more than doubled the sample to a total of 23 GCs and we were able to successfully measure the rotation amplitude and the position angle of the rotation axis for 21 clusters. Moreover, the number of stars observed for each individual cluster varies from 26 to 215 in Szigeti et al. 2021, while it varies from 65 to 1864 in our work. Despite these differences in data, the methodology to investigate the rotation amplitude and the position angle of the rotational axis of the clusters (namely the second method described in Section 3) is similar, thus it is possible to compare the results of the two works.

As noted from the Table 2, the comparison between our results and those reported in literature works shows some discrepancies. In particular, even for the best-studied case (NGC 5139 with 1864 stars), the results are not always consistent with the literature. As regards the rotation amplitude, there is a factor of ~ 2 discrepancy present in almost every cluster. This can be explained by considering that the rotation amplitude is usually taken to be half of the amplitude of the sinusoidal function (see for example Lane et al. 2011 and Szigeti et al. 2021). Even the position angle of the rotational axis values in this work are different from those reported in the literature. Some of these discrepancies (especially for the clusters with a lower number of stars) can be explained by different field of view used in the data (e.g. Kamann et al. 2018 focuses on more central FoVs) or different data used (e.g. Sollima et al. 2019 derives 3D rotation amplitudes from proper motion and line-of-sight

velocity simultaneously), or lack of perspective correction (e.g. van de Ven et al. 2006). However, other effects may also be responsible for the discrepancies between this work and those of the literature (and in some cases also between one literature work and another). The first depends on the observed patterns and the definition of the best-fit sine function that fits these points. A different position of the observed patterns or different fit of the sine function can lead to discrepant results. As in the case of NGC 5139 (ω Cen) that does not show a minimum or maximum position in the best-fit sine function at low values of PA (as shown instead in the work of Bianchini et al. 2013), but the minimum or maximum is present to higher values of PA. This can explain the high PA_0 value obtained in this work compared to the other literature work⁷. The same applies to the globular cluster NGC 6205, in which the work of Szigeti et al. 2021 notes a minimum position at lower PA, while in this work it is to higher PA values. In both of these cases, the observed patterns, and consequently the best fits, are similar to those reported in the literature works, but with a shift which varies the PA_0 results. A different situation is that of the globular clusters NGC 2808, NGC 3201, NGC 5904 and NGC 7078. In this case, the position of the observed patterns and the definition of the best-fit sine function are definitely divergent from those reported in the literature, causing discrepancies in PA_0 values. Furthermore, although the same method and the convention $PA\ 90 =$ East anti-clockwise system were used to define the observed patterns and the best-fit sine function, different approaches have been adopted to determine PA_0 in different works. For instance,

⁷ A high position angle value has also been derived in van de Ven et al. 2006 for ω Cen. In this work, the position angle has been defined as the angle between the observed major axis and North (measured counterclockwise through East) and determined by fitting elliptic isophotes to the smoothed Digital Sky Survey (DSS) image of the cluster, while keeping the centre fixed. In this way, the position angle is about 100° , a value discrepant to other values reported in the literature.

Ferraro et al. 2018 consider only the minimum position in the best-fit sine function to derive the PA_0 for the globular clusters NGC 5272, NGC 3201, NGC 0362, NGC 6171, NGC 6254, whereas this work takes into account both the minimum and maximum position (the same method used in Szigeti et al. 2021). Instead, Lardo et al. 2015 consider only the maximum position in the best-fit sine function for the clusters NGC 2808, NGC 6752, NGC 7078 and NGC 1851. Another method is the one used by Bellazzini et al. 2012 which derives the PA_0 value from the best-fit equation using the formula $\phi = 270 - PA_0$ (where ϕ is the phase of best-fit sine function) for the globular clusters NGC 5904, NGC 2808, NGC 7078, NGC 1851, NGC 6171, NGC 6254 and NGC 6388. All these effects mentioned above may be responsible for the discrepancies in PA_0 between this work and those in the literature.

The last comparison with the literature regards the two GCs, NGC 6218 and NGC 6838, that do not show a coherent sinusoidal pattern in the figures⁸ derived from the second method described in Section 3 (see Appendix B). Consequently, there is no clear sign of rotation for these two clusters and for these clusters, it was not possible to measure A_{rot} (neither with the best-fit sine function nor with the peak-to-peak approach, see section 3) and PA_0 . In the literature, both clusters have been studied by Bellazzini et al. 2012, Kimmig et al. 2015 and Bianchini et al. 2018 and in these works, they found a signature of rotation. As explained in Bellazzini et al. 2012, a work that uses the same adopted technique in this analysis, the results may also suffer from biases associated with the dimension of the samples for each GCs and with the radial distribution of sample stars. Moreover, the data used in Bellazzini et al. 2012, Kimmig et al. 2015 and Bianchini et al. 2018 come from FLAMES-GIRAFFE sample, Hectochelle on the MMT telescope, and Gaia DR2 respectively, while the data of this work come from APOGEE-2 DR17 and Gaia (EDR3). Therefore, more observational data are required to verify the presence of systemic rotation in the GCs NGC 6218 and NGC 6838.

4.2. General considerations

Below are two interesting considerations regarding the available data and possible effects that could influence the detection of the systemic rotation in the GCs.

An important effect that can produce a non-negligible amount of apparent rotation is the perspective rotation. It is particularly relevant for GCs that have a large extent on the plane of the sky. For example, for NGC 5139 (ω Cen), this effect can be extremely relevant (see for example Merritt et al. 1997 and van de Ven et al. 2006). Indeed, as reported in van de Ven et al. 2006, for the data typically extending to 20 arcmin from the ω Cen cluster centre, the maximum amplitude of the perspective rotation for the proper motions is about 0.06 mas yr^{-1} and for the line-of-sight velocity about 0.8 km s^{-1} . These values are a significant fraction of the observed mean velocities shown in this literature work, so the perspective rotation cannot be ignored. For this reason, we calculated the perspective rotation for ω Cen, which is the GC with the largest extent on the plane of the sky in our sample of clusters, using our available data

⁸ The reference figures are those that show the difference between the mean velocities on each side of a cluster with respect to a line passing through the cluster center with a position angle PA (measured from north to east, north = 0° , east = 90° , clockwise system), as a function of the adopted PA.

and the technique described in van de Ven et al. 2006. As PA_0 we considered the value derived in this work, namely 162° . To derive the values of the perspective rotation for each star, we applied Eq. 6 reported in the reference literature work, adopting the canonical distance of 5 kpc and the systemic motion given in Eq. 3 from the reference work. The perspective rotation of each star is insignificant compared to its \tilde{V}_r , so it could be ignored. Nevertheless, we corrected the observed stellar velocities by subtracting it. As a result, the kinematic data corrected for perspective rotation return a A_{fit} value of 13.69 km/s (instead of 13.85 km/s without correction) and a $A_{peak-peak}$ value of 13.32 km/s (instead of 12.98 km/s). The difference between the values with and without correction is extremely low, so the effect of perspective rotation is negligible. Since this effect is inappreciable for ω Cen and all the other clusters analyzed in this work have a Jacobi radius, which is considered as a parameter for the size of the field of view sampled, lower than that of ω Cen (see Table 1), in this work, we did not correct the observed velocities for perspective rotation.

The strategy to use the fitting of a sine law is commonly used to detect rotation from resolved kinematics. It is a reasonably good method to estimate the PA of the rotation axis. However, for the estimation of the rotation amplitude, it presents a major drawback. Indeed, given that GCs are characterized by differential rotation curves, the value of the rotation amplitude measured with this method strongly depends on the spatial distribution of the line-of-sight velocity samples. A differential rotation profile of a GC usually peaks around 1-2 half-light radii. Therefore, if the data do not sample this region, they will systematically show a lower rotation value, and vice versa if they are concentrated around these intermediate regions. Nevertheless, as demonstrated for example in Lanzoni et al. 2018, which tests the variability of their results considering different radii, the rotation amplitude and the position angle of the rotation axis are essentially constant in all of the investigated radii, as expected in the case of a coherent global rotation of the system. In this reference work, the authors considered a set of concentric annuli around the cluster center of NGC 5904, avoiding the innermost region, where the statistic is poor, and the outermost region, where the sampling is scant and nonsymmetric. As a result of this test (see Table 2 and Figure 7 of the reference paper), the values of A_{rot} and PA_0 are very similar between the annulus and the other. For this reason, since we consider the case of a coherent global rotation for each GC, in this work we did not carry out a test on the variability of the results at different radii.

5. Conclusions

In this work, 23 globular clusters have been studied to verify the presence or not of systemic rotation. Below are the main conclusions of this analysis:

- Using the data and methods described in this analysis, 21 GCs show a signature of systemic rotation. For these clusters, the rotation amplitude and the PA of the rotation axis were calculated. As a result, the clusters cover a remarkable range of rotational amplitudes, from $\sim 0.77 \text{ km/s}$ to $\sim 13.85 \text{ km/s}$. In particular, the clusters that exhibit highest rotation are NGC 5904, NGC 5139 and NGC 0104.

Table 2. Comparison with literature values. The first sub-column represents the rotation amplitude in km/s and the second is the position angle of the rotational axis in degrees. The last row contains the values of this analysis, which represent the values of the observed rotation. Since different conventions of PA_0 were followed, the published result have been converted to $PA_0 = 90^\circ = \text{East}$, anti-clockwise system.

Reference	NGC 5139		NGC 6715		NGC 0104		NGC 5272	
	A_{rot}	PA_0	A_{rot}	PA_0	A_{rot}	PA_0	A_{rot}	PA_0
Lane et al. 2010b	-	-	-	-	2.2±0.2	-	-	-
Bellazzini et al. 2012	6.0±1.0	-	2.0±0.5	-	4.4±0.4	-	-	-
Bianchini et al. 2013	6.79	12±1	-	-	4.00	136±1	-	-
Fabricius et al. 2014	-	-	-	-	-	-	-	192.2±11.8
Kimmig et al. 2015	-	-	1.6±2.9	-	4.0±0.3	-	0.6±1.0	-
Ferraro et al. 2018	-	-	-	-	-	-	1.0	151
Kamann et al. 2018	-	9.9±4.3	-	-	-	134.1±3.6	-	-
Sollima et al. 2019	4.27±0.52	9.8±7.6	0.57±1.11	-	5.00±0.32	135.7±4.6	1.75±0.42	-
Szigeti et al. 2021	-	-	-	-	-	-	1.19±0.3	164±15
This work	13.85±0.25	162	6.01±0.18	252	9.16±0.50	216	2.46±0.12	162

Reference	NGC 6656		NGC 3201		NGC 5904		NGC 6121	
	A_{rot}	PA_0	A_{rot}	PA_0	A_{rot}	PA_0	A_{rot}	PA_0
Lane et al. 2010b	1.5±0.4	-	-	-	-	-	0.9±0.1	70–250
Bellazzini et al. 2012	1.5±0.4	-	1.2±0.3	-	2.6±0.5	157	1.8±0.2	-
Fabricius et al. 2014	-	-	-	-	-	148.5±5.6	-	-
Kimmig et al. 2015	2.5±2.3	-	-	-	2.1±0.7	-	1.3±0.5	-
Lee 2017	-	-	-	-	3.36±0.7	128	-	-
Ferraro et al. 2018	-	-	1.3	215	-	-	-	-
Lanzoni et al. 2018	-	-	-	-	4.0	145	-	-
Kamann et al. 2018	-	280.9±23.9	-	244.3±188.9	-	305.7±20.3	-	214.5±9.4
Sollima et al. 2019	3.38±0.71	107.2±9.2	0.80±0.41	-	4.11±0.42	138.4±6.0	0.22±0.17	-
Szigeti et al. 2021	-	-	-	-	3.45±0.4	148±6	-	-
This work	5.75±0.06	252	3.37±0.10	324	8.03±0.14	198	2.70±0.08	234

Reference	NGC 2808		NGC 6205		NGC 6752		NGC 6397	
	A_{rot}	PA_0	A_{rot}	PA_0	A_{rot}	PA_0	A_{rot}	PA_0
Lane et al. 2010b	-	-	-	-	≤ 0.2	-	-	-
Bellazzini et al. 2012	3.3±0.5	152	-	-	0.0±0.0	-	0.2±0.5	-
Fabricius et al. 2014	-	-	-	196.5±7.8	-	-	-	-
Lardo et al. 2015	4.72±0.2	270	-	-	0.67±0.2	200	-	-
Kimmig et al. 2015	3.1±3.8	-	-	-	0.3±0.5	-	-	-
Cordero et al. 2017	-	-	2.7±0.9	14±19	-	-	-	-
Kamann et al. 2018	-	313.0±2.4	-	-	-	139.1±41.8	-	-
Sollima et al. 2019	2.25±0.56	143.9±8.4	1.53±0.61	14.5±14.2	0.91±0.34	-	0.48±0.17	171.4±15.6
Szigeti et al. 2021	-	-	2.38±0.4	26±9	-	-	-	-
This work	8.42±0.34	198	5.62±0.17	306	1.04±0.15	162	1.39±0.08	198

Reference	NGC 7078		NGC 0362		NGC 1851		NGC 6171	
	A_{rot}	PA_0	A_{rot}	PA_0	A_{rot}	PA_0	A_{rot}	PA_0
Bellazzini et al. 2012	3.8±0.5	290	-	-	1.6±0.5	252	2.9±1.0	264
Bianchini et al. 2013	2.84	106±1	-	-	-	-	-	-
Lardo et al. 2015	3.63±0.1	120	-	-	1.65±0.5	50	-	-
Kimmig et al. 2015	2.5±0.8	-	1.6±1.4	-	-	-	-	-
Ferraro et al. 2018	-	-	1.1	260	-	-	1.2	167
Kamann et al. 2018	-	150.9±10.4	-	318.0±117.6	-	3.2±3.5	-	-
Sollima et al. 2019	3.29±0.51	127.4±28.8	0.51±0.56	-	0.45±0.42	-	0.70±0.46	-
Szigeti et al. 2021	2.38±0.4	120±11	-	-	-	-	0.72±0.3	168±30
This work	4.16±0.10	234	3.57±0.08	234	5.59±0.13	180	0.77±0.09	234

Reference	NGC 6254		NGC 6273		NGC 6341		NGC 6809	
	A_{rot}	PA_0	A_{rot}	PA_0	A_{rot}	PA_0	A_{rot}	PA_0
Lane et al. 2010b	-	-	-	-	-	-	0.25±0.09	-
Bellazzini et al. 2012	0.4±0.5	95	-	-	-	-	0.5±0.2	-
Fabricius et al. 2014	-	153.5±14.7	-	-	-	98.9±12.0	-	-
Kimmig et al. 2015	-	-	-	-	1.8±0.8	-	0.4±0.2	-
Johnson et al. 2017	-	-	3.83±0.12	126±2	-	-	-	-
Ferraro et al. 2018	1.4	315	-	-	-	-	-	-
Kamann et al. 2018	-	142.8±17.9	-	-	-	-	-	-
Sollima et al. 2019	0.26±0.56	-	4.19±1.12	123.1±13.2	1.46±0.61	-	0.88±0.38	-
Szigeti et al. 2021	-	-	-	-	2.06±0.6	154±14	-	-
This work	2.27±0.16	198	2.37±0.22	270	4.18±0.11	216	3.58±0.10	252

Reference	NGC 6388	
	A_{rot}	PA_0
Bellazzini et al. 2012	3.9±1.0	117
Kamann et al. 2018	-	318.2±16.8
Sollima et al. 2019	1.51±0.65	-
This work	6.64±0.47	270

- Two different methods have been used to calculate the rotation amplitude: the best-fit sine function and the peak-to-peak methods. A comparison between the two methods shows they give similar results, within the uncertainties.
- The comparison with the literature shows that in general our measurements are consistent with previously published rotation values.

In conclusion, most if not all of the present-day GCs show measurable rotation. Processes like interactions can induce rotation in some individual cases, but it is very difficult to spin up individually the whole population of such massive objects ($> 10^4 M_{\odot}$). Therefore we surmise that this trait was probably imprinted initially, during the epoch of their process of formation (see for example Kamann et al. 2018 and Bianchini et al. 2018). With the advent of large spectroscopic surveys like 4MOST (Chiappini et al. 2019) and WEAVE (Jin et al. 2023), it would be possible to explore in more detail the rotational properties of larger homogeneous GCs samples.

Acknowledgements.

I.P. acknowledges support from ANID BECAS/DOCTORADO NACIONAL 21230761.

J.G.F-T acknowledges support provided by Agencia Nacional de Investigación y Desarrollo de Chile (ANID) under the Proyecto Fondecyt Iniciación 2022 Agreement No. 11220340, and from ANID under the Concurso de Fomento a la Vinculación Internacional para Instituciones de Investigación Regionales (Modalidad corta duración) Agreement No. FOVI210020, and from the Joint Committee ESO-Government of Chile 2021 under the Agreement No. ORP 023/2021, and from Becas Santander Movilidad Internacional Profesores 2022, Banco Santander Chile, and from Vicerrectoría de Investigación y Desarrollo Tecnológico (VRIDT) at Universidad Católica del Norte under resolución No. 061/2022-VRIDT-UCN.

D.M. gratefully acknowledges support from the ANID BASAL projects ACE210002 and FB210003, from Fondecyt Project No. 1220724, and from CNPq Project 350104/2022-0.

References

- Abdurro'uf, Accetta, K., Aerts, C., et al. 2022, *ApJS*, 259, 35, doi: 10.3847/1538-4365/ac4414
- Alfaro-Cuello, M., Kacharov, N., Neumayer, N., et al. 2020, *ApJ*, 892, 20, doi: 10.3847/1538-4357/ab77bb
- Bellazzini, M., Bragaglia, A., Carretta, E., et al. 2012, *A&A*, 538, A18, doi: 10.1051/0004-6361/201118056
- Bellini, A., Bianchini, P., Varri, A. L., et al. 2017, *ApJ*, 844, 167, doi: 10.3847/1538-4357/aa7c5f
- Bellini, A., Vesperini, E., Piotto, G., et al. 2015, *ApJL*, 810, L13, doi: 10.1088/2041-8205/810/L13
- Bellini, A., Libralato, M., Bedin, L. R., et al. 2018, *ApJ*, 853, 86, doi: 10.3847/1538-4357/aaa3ec
- Bianchini, P., van der Marel, R. P., del Pino, A., et al. 2018, *MNRAS*, 481, 2125, doi: 10.1093/mnras/sty2365
- Bianchini, P., Varri, A. L., Bertin, G., & Zocchi, A. 2013, *ApJ*, 772, 67, doi: 10.1088/0004-637X/772/1/67
- Boberg, O. M., Vesperini, E., Friel, E. D., Tiongco, M. A., & Varri, A. L. 2017, *ApJ*, 841, 114, doi: 10.3847/1538-4357/aa7070
- Chiappini, C., Minchev, I., Starkenburg, E., et al. 2019, *The Messenger*, 175, 30, doi: 10.18727/0722-6691/5122
- Cordero, M. J., Hénault-Brunet, V., Pilachowski, C. A., et al. 2017, *MNRAS*, 465, 3515, doi: 10.1093/mnras/stw2812
- Cordoni, G., Milone, A. P., Mastrobuono-Battisti, A., et al. 2020a, *ApJ*, 889, 18, doi: 10.3847/1538-4357/ab5aee
- Cordoni, G., Milone, A. P., Marino, A. F., et al. 2020b, *ApJ*, 898, 147, doi: 10.3847/1538-4357/aba04b
- Cote, P., Welch, D. L., Fischer, P., & Gebhardt, K. 1995, *ApJ*, 454, 788, doi: 10.1086/176532
- Dalessandro, E., Raso, S., Kamann, S., et al. 2021, *MNRAS*, 506, 813, doi: 10.1093/mnras/stab1257
- de Vita, R., Bertin, G., & Zocchi, A. 2016, *A&A*, 590, A16, doi: 10.1051/0004-6361/201628274
- Einsel, C., & Spurzem, R. 1999, *MNRAS*, 302, 81, doi: 10.1046/j.1365-8711.1999.02083.x
- Ernst, A., Glaschke, P., Fiestas, J., Just, A., & Spurzem, R. 2007, *MNRAS*, 377, 465, doi: 10.1111/j.1365-2966.2007.11602.x
- Fabrizius, M. H., Noyola, E., Rukdee, S., et al. 2014, *ApJ*, 787, L26, doi: 10.1088/2041-8205/787/L26
- Ferraro, F. R., Mucciarelli, A., Lanzoni, B., et al. 2018, *ApJ*, 860, 50, doi: 10.3847/1538-4357/aabe2f
- Gaia Collaboration, Brown, A. G. A., Vallenari, A., et al. 2021, *A&A*, 649, A1, doi: 10.1051/0004-6361/202039657
- Gieles, M., & Zocchi, A. 2015, *MNRAS*, 454, 576, doi: 10.1093/mnras/stv1848
- Giersz, M., & Heggie, D. C. 2011, *MNRAS*, 410, 2698, doi: 10.1111/j.1365-2966.2010.17648.x
- Holtzman, J. A., Hasselquist, S., Shetrone, M., et al. 2018, *AJ*, 156, 125, doi: 10.3847/1538-3881/aad4f9
- Hong, J., Kim, E., Lee, H. M., & Spurzem, R. 2013, *MNRAS*, 430, 2960, doi: 10.1093/mnras/stt099
- Jeffreson, S. M. R., Sanders, J. L., Evans, N. W., et al. 2017, *MNRAS*, 469, 4740, doi: 10.1093/mnras/stx1152
- Jin, S., Trager, S. C., Dalton, G. B., et al. 2023, *MNRAS*, doi: 10.1093/mnras/stad557
- Johnson, C. I., Caldwell, N., Rich, R. M., et al. 2017, *ApJ*, 836, 168, doi: 10.3847/1538-4357/836/2/168
- Kacharov, N., Bianchini, P., Koch, A., et al. 2014, *A&A*, 567, A69, doi: 10.1051/0004-6361/201423709
- Kamann, S., Husser, T. O., Dreizler, S., et al. 2018, *MNRAS*, 473, 5591, doi: 10.1093/mnras/stx2719
- Kamlah, A. W. H., Spurzem, R., Berczik, P., et al. 2022, *MNRAS*, 516, 3266, doi: 10.1093/mnras/stac2281
- Kim, E., Yoon, I., Lee, H. M., & Spurzem, R. 2008, *MNRAS*, 383, 2, doi: 10.1111/j.1365-2966.2007.12524.x
- Kimmig, B., Seth, A., Ivans, I. I., et al. 2015, *AJ*, 149, 53, doi: 10.1088/0004-6256/149/2/53
- King, I. R. 1966, *AJ*, 71, 64, doi: 10.1086/109857
- Lane, R. R., Kiss, L. L., Lewis, G. F., et al. 2011, *A&A*, 530, A31, doi: 10.1051/0004-6361/201116660
- Lane, R. R., Brewer, B. J., Kiss, L. L., et al. 2010a, *ApJ*, 711, L122, doi: 10.1088/2041-8205/711/L122
- Lane, R. R., Kiss, L. L., Lewis, G. F., et al. 2010b, *MNRAS*, 406, 2732, doi: 10.1111/j.1365-2966.2010.16874.x
- Lanzoni, B., Mucciarelli, A., Origlia, L., et al. 2013, *ApJ*, 769, 107, doi: 10.1088/0004-637X/769/2/107
- Lanzoni, B., Ferraro, F. R., Mucciarelli, A., et al. 2018, *ApJ*, 861, 16, doi: 10.3847/1538-4357/aac26a
- Lardo, C., Pancino, E., Bellazzini, M., et al. 2015, *A&A*, 573, A115, doi: 10.1051/0004-6361/201425036
- Lee, J.-W. 2017, *ApJ*, 844, 77, doi: 10.3847/1538-4357/aa7b8c
- Lee, Y.-N., & Hennebelle, P. 2016, *A&A*, 591, A30, doi: 10.1051/0004-6361/201527981
- Libralato, M., Vesperini, E., Bellini, A., et al. 2023, *ApJ*, 944, 58, doi: 10.3847/1538-4357/acaec6
- Livernois, A., Vesperini, E., Tiongco, M., Varri, A. L., & Dalessandro, E. 2021, *MNRAS*, 506, 5781, doi: 10.1093/mnras/stab2119
- Livernois, A. R., Vesperini, E., Varri, A. L., Hong, J., & Tiongco, M. 2022, *MNRAS*, 512, 2584, doi: 10.1093/mnras/stac651
- Majewski, S. R., APOGEE Team, & APOGEE-2 Team. 2016, *Astron. Nachr.*, 337, 863, doi: 10.1002/asna.201612387
- Majewski, S. R., Schiavon, R. P., Frinchaboy, P. M., et al. 2017, *AJ*, 154, 94, doi: 10.3847/1538-3881/aa784d
- Mapelli, M. 2017, *MNRAS*, 467, 3255, doi: 10.1093/mnras/stx304
- Merritt, D., Meylan, G., & Mayor, M. 1997, *AJ*, 114, 1074, doi: 10.1086/118538
- Pancino, E., Galfo, A., Ferraro, F. R., & Bellazzini, M. 2007, *ApJ*, 661, L155, doi: 10.1086/518959
- Richer, H. B., Heyl, J., Anderson, J., et al. 2013, *ApJL*, 771, L15, doi: 10.1088/2041-8205/771/L15
- Scalco, M., Livernois, A., Vesperini, E., et al. 2023, *MNRAS*, 522, L61, doi: 10.1093/mnras/slada042
- Schiavon, R. P., Phillips, S. G., Myers, N., et al. 2023, *MNRAS*, doi: 10.1093/mnras/stad3020
- Sollima, A., Baumgardt, H., & Hilker, M. 2019, *MNRAS*, 485, 1460, doi: 10.1093/mnras/stz505
- Sollima, A., Bellazzini, M., Smart, R. L., et al. 2009, *MNRAS*, 396, 2183, doi: 10.1111/j.1365-2966.2009.14864.x
- Szigeti, L., Mészáros, S., Szabó, G. M., et al. 2021, *MNRAS*, 504, 1144, doi: 10.1093/mnras/stab1007
- Tiongco, M. A., Vesperini, E., & Varri, A. L. 2017, *MNRAS*, 469, 683, doi: 10.1093/mnras/stx853
- . 2018, *MNRAS*, 475, L86, doi: 10.1093/mnras/sly009
- . 2022, *MNRAS*, 512, 1584, doi: 10.1093/mnras/stac643
- van de Ven, G., van den Bosch, R. C. E., Verolme, E. K., & de Zeeuw, P. T. 2006, *A&A*, 445, 513, doi: 10.1051/0004-6361:20053061
- van den Bergh, S. 2008, *AJ*, 135, 1731, doi: 10.1088/0004-6256/135/5/1731
- Varri, A. L., & Bertin, G. 2012, *A&A*, 540, A94, doi: 10.1051/0004-6361/201118300
- Vasiliev, E., & Baumgardt, H. 2021, *MNRAS*, 505, 5978, doi: 10.1093/mnras/stab1475
- Vesperini, E., Varri, A. L., McMillan, S. L. W., & Zepf, S. E. 2014, *MNRAS*, 443, L79, doi: 10.1093/mnras/slu088
- Wilson, C. P. 1975, *AJ*, 80, 175, doi: 10.1086/111729

Appendix A: PA_0 conversions

This Appendix includes the details of the conversions of the position angle of the rotation axis values reported in the works of Fabricius et al. 2014, Cordero et al. 2017, Kamann et al. 2018, and Sollima et al. 2019 into the north, $PA = 0^\circ$, to east, $PA = 90^\circ$, anti-clockwise system (traditional reference system). In each case, PA_0 is the final position angle of the rotation axis used in this paper, after conversion into the north, $PA = 0^\circ$, to east, $PA = 90^\circ$, anti-clockwise system, and $PA_{0,*}$ is the position angle of the rotation axis reported in the studies listed above.

- In Fabricius et al. 2014, the kinematic position angle has been obtained from the velocity field. Since the values of $PA_{0,*}$ of GCs in common with this work cover between 0° and 180° , the value of PA_0 in the traditional reference system is equal to the sum of the $PA_{0,*}$ and 90° .
- In the case of Cordero et al. 2017, the value of the PA_0 is that converted and reported in Szigeti et al. 2021.
- In Kamann et al. 2018, the values of PA_0 are written in the $PA = 0^\circ$, to east, $PA = 90^\circ$, anti-clockwise system. However, the range of $PA_{0,*}$ values does not cover from 0° to 360° (where all values are positive). Indeed, in this work, the ranges of $PA_{0,*}$ values are between $[0^\circ, 180^\circ]$, $[-180^\circ, -0^\circ]$. Therefore, to convert the reported values, the following algorithm is used:
 - If $0^\circ < PA_{0,*} < 180^\circ$, then the value of PA_0 in the traditional reference system is equal to $PA_{0,*}$;
 - If $0^\circ < PA_{0,*} < -180^\circ$ (namely $180^\circ < PA_0 < 360^\circ$ in the traditional reference system), then $PA_0 = 360^\circ - |PA_{0,*}|$
- Sollima et al. 2019 used the convention from north, $PA = 0^\circ$, to west, $PA = 90^\circ$, anti-clockwise system. Therefore, in this case the following algorithm is used:
 - If $0^\circ < PA_{0,*} < 180^\circ$, then the value of PA_0 in the traditional reference system is $180^\circ - PA_{0,*}$
 - Otherwise, if $PA_{0,*} > 180^\circ$, then the value of PA_0 in the traditional reference system is $360^\circ - PA_{0,*}$

Appendix B: GCs without signature of systemic rotation

This Appendix reports the difference between the mean radial velocities located on each side of the cluster with respect to a line passing through the center as a function of PA (measured from north, $PA = 0^\circ$, to east, $PA = 90^\circ$, clockwise system) as a function of the adopted PA, for the globular clusters NGC 6218 and NGC 6838. These figures do not show coherent sinusoidal behavior of the observed patterns (blue dots), thus these clusters do not show a signature of systemic rotation.

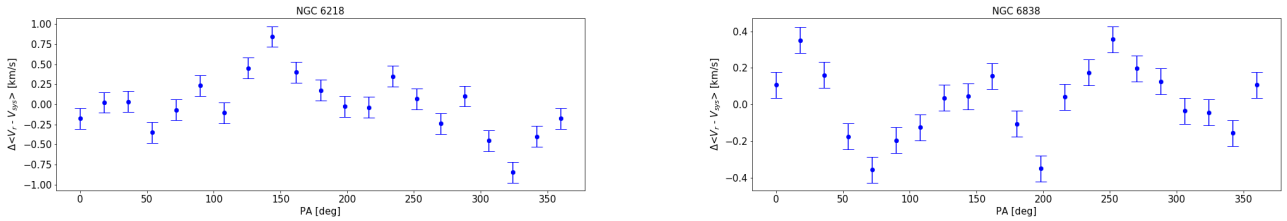


Fig. B.1. Left: NGC 6218. Right: NGC 6838.

Appendix C: Test to assess step value

This Appendix explores the choice of using a step of 18° in the second and third methods described in Section 3 to calculate the A_{rot} and PA_0 . Indeed, especially the peak-to-peak approach is very likely strongly affected by statistical scatter due to the determination of the peak and by the steps in degree used for the construction of the curves. Therefore, the value of 18° , used for all clusters, might seem rather large, especially for those GCs, such as NGC 5139, where a large number of line-of-sight velocities are available. For these reasons, we investigate the dependence of our results on the step chosen to demonstrate the robustness of our methods.

This appendix shows the results obtained for the NGC 5139 cluster, which is the GC with the highest number of available stars, using the same methods adopted in our analysis and described in Section 3, but with a step of 9° . The signature of systemic rotation using a step of 9° for this cluster is shown in Figure C.1, while the A_{rot} and PA_0 obtained using this step and the comparison with the results obtained with a step of 18° is shown in the Table C.1.

As a result, the use of these two different steps gives equivalent values of A_{rot} and PA_0 . Therefore, the use of a step of 18° for all the clusters is a reasonable choice. Indeed, it allows us to consider a significant number of stars for each range in the case of clusters with a low number of available stars. Whereas, in the case of GCs with a high number of available stars, the use of this step does not show a significant difference in the results.

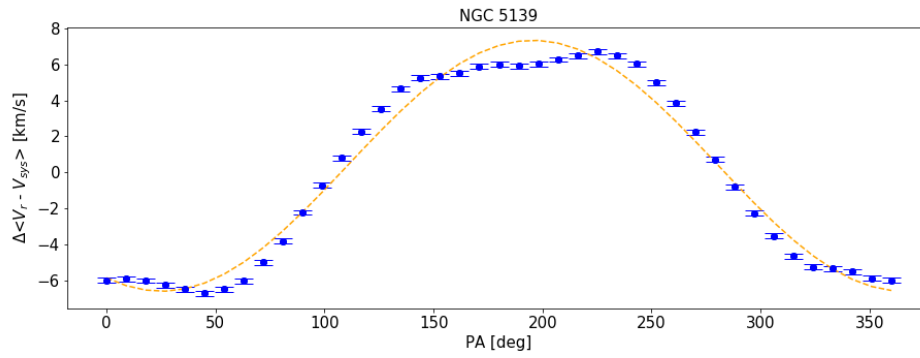


Fig. C.1. Difference between the mean radial velocities located on each side of the cluster with respect to a line passing through the center as a function of PA (measured from north, PA = 0°, to east, PA = 90°, with a step of 9°, clockwise system) as a function of the adopted PA, for the globular cluster NGC 5139. The orange dashed line is the sine function that best fits the observed patterns (blue dots).

Table C.1. Comparison of the results obtained using a step of 18° and a step of 9° for the globular cluster NGC 5139.

NGC 5139		
	Step of 18°	Step of 9°
A_{fit}	13.85 ± 0.25	13.94 ± 0.17
$A_{peak-peak}$	12.98 ± 0.29	13.43 ± 0.20
PA_0	162	162